SRAM-based heavy ion beam flux and LET dosimetry

Andrea Coronetti, *Associate Member, IEEE*, Rubén García-Alía, *Member, IEEE*, Luigi Dilillo, *Member, IEEE*, Carolina Imianosky, Douglas Almeida dos Santos, Lucas Matana Luza, Alexandre Bosser, Kacper Bilko, Andreas Waets, Karolina Klimek, and Frédéric Saigné.

***Abstract*—This paper explores the possibility of enhancing the capability of static random access memories (SRAMs) as heavy ion beam detectors starting from the multiple-cell upsets (MCUs) measured in some well characterized beams. In particular, the two main enablers brought by the MCU analysis are (1) the determination of the beam flux even when the LET of the beam is not known [whenever the LET is > 10 MeV/(mg/cm^2)] and (2) the estimation of the LET of the heavy ion beam without reliance on any other instrument. The methods designed to determine these quantities are explained in the paper and are calibrated using well characterized heavy ion beams. They are then put to test in less known heavy ion beams. Overall, the flux estimation, which exploits the saturation of the coverage, i.e., the ratio between MCU and beam fluence, instead of the unsaturated SEU cross section, can point out issues with beam calibration that can be corrected by the facility. The LET estimation, for which two different methods are proposed, when compared to Monte-Carlo simulations, showed a general agreement with an uncertainty of $\sim$3 MeV/(mg/cm^2), which is acceptable for typical measurements in which the LET data-points are spread by a larger range.**

***Index Terms*—Heavy ions, SEU, MCU, SRAM, dosimetry, facility, LET.**

I. Introduction

STATIC random access memories (SRAMs) are characterized by an array of sensitive cells spread over a broad surface that make them usable as cost-efficient beam and radiation environment monitors. SRAMs provide digitized information on the energy that a beam is depositing in a sensitive volume (SV). Therefore, if the charge deposited and collected does not exceed the critical charge, the information of the particle interaction is not captured. Vice versa, if the charge deposited and collected exceeds the critical charge, an upset is recorded, but any information about the charge in excess of the critical charge is also not captured.

The use of SRAMs as radiation monitors has been limited to a restricted amount of applications. One such use is that of flux monitoring. This can exploit either single-event upset (SEU) or single-event latchup (SEL) sensitivity [1–4]. It is achieved by measuring the SEU or SEL cross section as a function of the linear energy transfer (LET) of ions and by making use of this response as a calibration curve. When the LET of the beam is known one can estimate the flux by means of:

$$\dot{\Phi} = \frac{N_{SEE}}{\sigma(LET)} \tag{1}$$

Nevertheless, this can only be used when the LET of the beam is identified through independent dosimetry techniques, analytic calculations or numerical simulations.

In a similar vein, SRAMs have been installed on board satellites and used as radiation environment monitors for the space environment [5–19]. In this case, the further complication when it comes to determine the environmental flux is due to the exposure to a mixed-field of protons and ions that is generally not possible without knowing the single-event effect (SEE) response from both types of particles and without geolocalization of the events.

SRAMs have enabled these applications because they are inexpensive when compared to other detectors and also easy to program while providing millions of sensitive cells. However, one of the reason why it is not obvious to go beyond the flux monitoring capabilities is that the errors cannot be mapped to a physical position within the memory array. This is particularly the case for commercial SRAMs. Nowadays manufacturers perform a scrambling of the sensitive cells with respect to the way they are ordered inside a logical word. Typically, this descrambling algorithm is considered proprietary information for the manufacturer and is not released.

When this algorithm is available, an SRAM can become an even more powerful radiation monitor. One such example is the ESA Monitor [5]. The ESA Monitor is composed of four SRAMs based on 250 nm technology whose dies are arranged to cover a surface of 2×2 cm^2. Thanks to its large size

Manuscript received September 14^{th}, 2024.
This study has received funding from the European Union's Horizon 2020 research and innovation programme under the Marie Sklodowska Curie grant agreement no. 721624, the RADSAGA project, from the European Union's Horizon 2020 research and innovation programme under grant agreement no. 101008126, the RADNEXT project and from the European Union's Space Work Programme of the European Commission under agreement no. 101082402, the HEARTS project.

Andrea Coronetti (andrea.coronetti@gmail.com) was with CERN, CH-1211 Geneva, Switzerland and with Institute d'Électronique et des Systèmes, Université de Montpellier, 34090 Montpellier, France.

Rubén García Alía, Kacper Bilko, Andreas Waers and Karolina Klimek are with CERN, CH-1211 Geneva, Switzerland.

Luigi Dilillo are with LIRMM, Université de Montpellier, CNRS, 34095 Montpellier, France.

Lucas Matana Luza was with LIRMM, Université de Montpellier, 34095 Montpellier, France and is now with SENAI Innovation Institute in Embedded Systems, Florianopolis-SC, 88054-700, Brazil.

Carolina Imianosky and Douglas Almeida dos Santos are with Institute d'Électronique et des Systèmes, Université de Montpellier, 34090 Montpellier, France.

Alexandre Bosser was with LIRMM, Université de Montpellier, 34095 Montpellier, France, and is now with 3DPlus, 78530 Buc, France.

Frédéric Saigné is with Institute d'Électronique et des Systèmes, Université de Montpellier, 34090 Montpellier, France.

and the physical mapping of the SEUs, this detector allows assessing the uniformity of a beam [20, 21] over a typical surface of interest for component level testing with a single irradiation.

Strictly speaking, this capability can also be achieved when the mapping is not available. For instance, a single SRAM or an array of SRAMs with much smaller form factor can be scanned through the area containing the beam. This way one can obtain spatial information of the uniformity of a beam by comparing the SEE rates at different locations. The drawback is that it takes a much larger amount of time to achieve the same result as an ESA Monitor.

The purpose of this paper is to make use of the information about the physical location of the SEUs to further enable the capabilities of SRAMs as radiation monitors. This relies on the analysis of multiple-cell upsets (MCUs) caused by ion beams. MCUs occur whenever the energy deposited by a single-particle is not collected solely at the cell where the particle has struck, but is diffused and collected at the sensitive nodes of other physically adjacent or electrically connected cells. As a result, a single particle strike can cause a large amount of bit-flips. This can be exploited because, nowadays, commercial SRAMs, based on deep sub-micron technologies, are dominated by MCUs when exposed to ion beams [22]. The mechanisms behind MCUs have been studied in previous publications [23–27].

MCUs are the reason why manufacturers employ address scrambling in their memory. This way, if an MCU occurs, the errors are not happening within the same logical word, but are scattered among many. Single errors are also easier to identify and correct by error correction codes (ECC). This paper will present which resources MCUs bring to determination of flux in a facility even when the LET is not known a priori. As a main result, the paper will also present how the MCUs can be used to provide a rather accurate estimation of the LET of an ion beam.

II. Data collection and calibration

The target SRAM in this work is the CY62167GE30-45ZXI, a 65 nm, 16 Mbit SRAM commercially available from Infineon. In this version, the SRAM has an embedded ECC, which was disabled for the purpose of this work. For all the experimental measurements reported hereafter the SRAM is biased at 3.3 V I/O and written with a checkerboard pattern. During the irradiations, the SRAM was read continuously at intervals of 2.5 s and, when errors were found, the flipped bits were rewritten to the correct pattern. All ion irradiations were performed on delidded samples and at normal incidence.

Data on the SRAMs were collected in a number of European heavy ion facilities, including RADEF [28], UMCG-PARTREC [29], GANIL [30], GSI [31] and HEARTS@CERN [32]. The SEU data for all experiments have been published before [31–33], except those from RADEF and HEARTS@CERN. Only the RADEF measurements were performed in vacuum. For all other facilities the measurements were performed in air and sometimes by making use of degraders, when primary energies exceeded 30 MeV/n.

TABLE I
List of ions used at RADEF.

Ion	Energy [MeV/n]	LET [MeV/(mg/cm^2)]
O	22	1.17
Ar	10	9.7
Fe	9.3	18.6
Kr	10	31.3
Xe	9.3	60
Au	10	85.6

TABLE II
List of Pb ion parameters used at HEARTS@CERN. The LET at the DUT is calculated with FLUKA.

Extracted energy [MeV/n]	PMMA thickness [mm]	LET [MeV/(mg/cm^2)]
1000	0	13.6
1000	10	14.3
1000	20	15.6
1000	30	18.0
1000	34	19.8
1000	38	22.7
1000	40	24.9
1000	40.5	25.7
1000	41	26.6
1000	41.5	27.6
1000	42	28.7
1000	42.5	30.1
1000	43	31.7
1000	43.5	33.7
1000	44	36.4
1000	44.5	40.2
750	0	17.6
750	10	22.3
750	12	24.4
750	14	27.8
750	16	34.2
750	18	59.7
650	0	21.8
800	0	16.3
950	0	13.6
1100	0	12.2
1250	0	11.4
1400	0	11.0
1550	0	10.7

The list of ions used at RADEF is presented in Table I. As is shown, the data collected at RADEF provide the broadest possible LET range that can be exploited for the purpose of this work. Concerning the data collected at CERN, this is a high-energy ion facility that currently operates on a single Pb ion mode. Nevertheless, the ion parameters can be varied easily by either energy tuning in the accelerator or by degrading the high-energy beam with Polymethylmethacrylate (PMMA) slabs of different thickness placed in front of the device under test (DUT). Due to the physics of charge deposition of Pb in silicon at GeV/n energy, the minimum LET is never lower than 10 MeV/(mg/cm^2), whereas the maximum LET can be tuned to reach Bragg peak values of up to 100 MeV/(mg/cm^2). Table II reports a list of the Pb ion parameters employed during the test campaign. The LET of the beam at the DUT were calculated through Monte-Carlo simulations with FLUKA [34–36] that take into account the material budget in the beamline as well as the degrader. Nevertheless, the energy spread caused by the interaction with the material of the beamline (about 5% in terms of full width

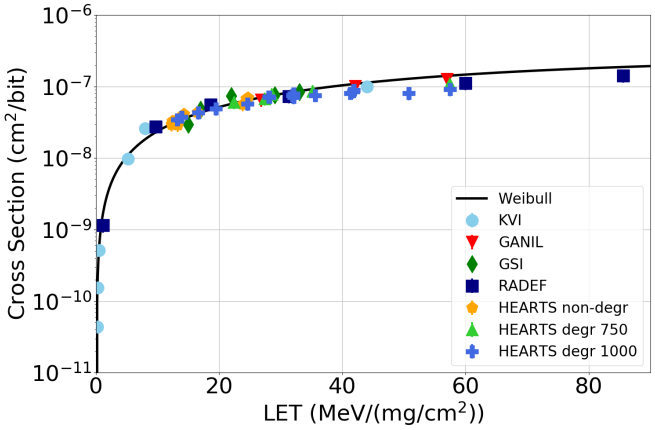

Fig. 1. SEU cross section as a function of LET for this memory measured at the five facilities.

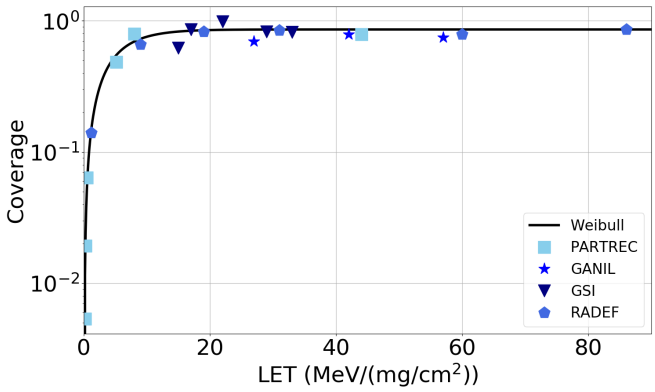

Fig. 2. Coverage or ratio between the MCUs and the fluence measurement provided by the facilities for data collected at various LETs.

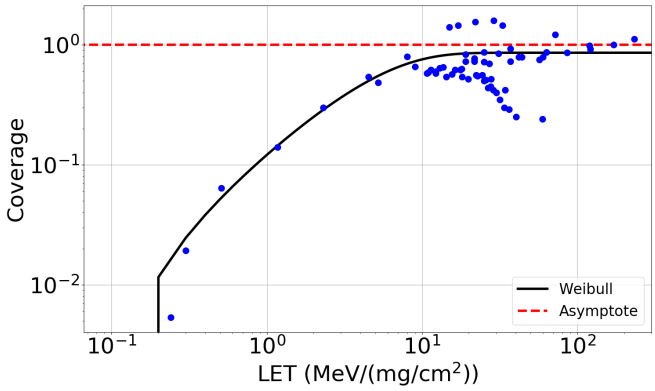

Fig. 3. Coverage resulting from the information provided by the facility about the fluence.

at half maximum) is not considered and, in the simulation, the beam is considered fully uniform before interacting with the degrader. For the calculation of the SEU cross section in this facility, the flux and fluence are obtained through a secondary emission chamber which is calibrated with a silicon diode [37].

The SEU cross sections measured at the five facilities are shown in Fig. 1 as a function of the LET of the beam. These data have been collected over the course of five years. The device tested in the different facilities was not always the same physical chip, but different chips from the same lot datecode (1731). While introducing an uncertainty related to the device-to-device variability, this makes it easier for others to reproduce and reuse the findings and data here presented. The variability among facilities for same or similar LET is typically within $\pm 30\%$ and may not be related solely to device variability, but to the variegated facility dosimetry uncertainties. The Weibull curve used to fit the data has the following parameters: LET_0 = 0.15 MeV/(mg/cm^2), σ_{sat} = 2.6 $\times$ 10^{-7} cm^2/bit, W = 70 MeV/(mg/cm^2), s = 1.2. Note that in this figure the SEUs represent all single-bit flips irrespectively of whether they belong to MCUs or not. If this was the case, the SEU cross section would be saturating to the dimension of the single cell when the LET is high enough. On the other hand, it can be seen that between 10 and 90 MeV/(mg/cm^2) the SEU cross section increases of about a factor of 5. This effect is primarily due to the increase in multiplicity of the MCUs as the LET increases.

MCU data for this SRAM have been published before [31, 32]. Other than the physical-to-logical mapping algorithm, the MCU clustering follows the criteria defined in [38, 39]. Therefore, the maximum Manhattan distance is taken to be 3 in both positive and negative, vertical and horizontal directions. Time-wise, and in particular when the beam is continuous, clustering must also be done checking through consecutive readouts.

III. Flux measurements from MCUs when the LET is not known

The standard way to determine the flux of a beam from an SRAM is to make use of (1) while having a prior knowledge of the LET. This is because the SEU cross section can strongly vary with the LET of the beam and may never saturate if no information on MCUs is available, as seen in Fig. 1. So, good accuracy from this equation can be obtained only if the LET is known from another detector, or from theory or simulation, because the SEU cross section above 10 MeV/(mg/cm^2) can even vary of up to a factor of 5.

MCUs allow determining the flux for the LET interval above 10 MeV/(mg/cm^2) even if an independent LET measurement is not available. This is because, differently from the SEU cross section, the ratio between the amount of SBUs+MCUs [from hereon called N_{MCU}, mainly because the MCUs are 99.9% of the events at LET $>$ 10 MeV/(mg/cm^2), so there is negligible error in neglecting the SBUs] and the beam fluence saturates above 10 MeV/(mg/cm^2). This can be exploited to achieve a flux measurement that is independent on the LET for a very wide LET range. A first independent calibration must be done to assess the coverage, i.e., the ratio between the total number of MCUs and the beam fluence over the DUT area and independently measured by the facility. At the limit, this ratio can never be higher than 1. This is because a single ion strike cannot cause more than a cluster of bit flips. In order to calculate this ratio, one also needs to correct the fluence that is given by the facility in ions/cm^2 in units of ions/die. This is obtained by multiplying the former by the sensitive area of

the die. For this memory the active area of the die is estimated to be A_{die} = 13.16 mm^2 from construction analysis.

The ratio between the MCUs and the fluence per die is depicted in Fig. 2 for the measurements at the various facilities and is plotted as a function of LET. It is noted that for all the points the ratio is indeed not above the asymptotic limit of 1. However, the saturation occurs at a value of ∼0.86. This may be due to the fact that the die does not contain only sensitive cells.

What Fig. 2 shows is that, independently of the imprecision on the die surface, the coverage slightly varies around 0.86, but that this can be considered a saturation value occurring just above 10 MeV/(mg/cm^2). The Weibull curve used to fit the data has the following parameters: LET_0 = 0.15 MeV/(mg/cm^2), $Coverage_{sat}$ = 0.86, W = 5 MeV/(mg/cm^2), s = 1.1.

Due to this property, the SRAM becomes equivalent to an ion counter. As shown, since the coverage becomes independent on the LET above 10 MeV/(mg/cm^2), there is no further need to independently know the LET of a beam to be able to calculate the flux. In fact, for this memory, the ion flux or fluence will be simply determined as follows:

$$\dot{\Phi} = \frac{N_{MCU} \times Coverage_{sat}}{A_{die}} = 6.53 \times N_{MCU}[cm^{-2}] \quad (2)$$

Thanks to the capability introduced by the coverage, one can also assess whether the data provided by the facility in terms of fluence are consistent. Through the equation above, one can calculate the fluence as seen by the SRAM in units of ions/cm^2 and compare it with that provided by the facility. One such comparison is provided through Fig. 3. The figure depicts a number of measurements collected in different facilities. The data have been made anonymous. As one can see from the very high LETs, they also include some data collected with a tilt or roll angle (α). For these data, the points have been placed at the expected effective LET [LET_{eff} = LET/cos(α)]. The fluence provided by the facility was already corrected for the smaller aspect ratio.

As the figure shows, this technique can point out some discrepancies with respect to the fluence data provided by the facility, which can either be over- or underestimated. In some cases, the resulting coverage was higher than the maximum physical limit of 1. This pointed out that the way the fluence was calculated by the facility was providing an underestimation of the actual fluence received by the device. On the other hand, when the coverage is lower than expected, this is an indication of an overestimation of the fluence. This can be the case when degradation of the beam is introduced, resulting not only in a loss of energy of the ions, but also in a loss of flux. Another case is related to the calibration of instruments. Due to the degradation there is a spread in the energy that can result in a wider spectrum in terms of energy deposition in, for instance, a silicon diode. Determining where to cut this wider spectrum to provide the ion counting can provide better or worse estimations of the actual amount of ions seen by the DUT. In this case, better consistency was found when considering a narrower portion of the spectrum around the energy deposition peak. The data shown in the figure were those considering a wider portion of the spectrum around the peak that clearly show a large discrepancy. Thanks to the analysis performed on the SRAM it was possible to re-calibrate the flux received by the DUTs with a narrower peak that made the points realign with the saturation at 0.86. In this respect, the reliance on this verification tool was very instrumental for the final calibration of the diode at HEARTS@CERN. The new flux calibration values could then be used for the calculation of cross sections of other devices for which this analysis was not possible.

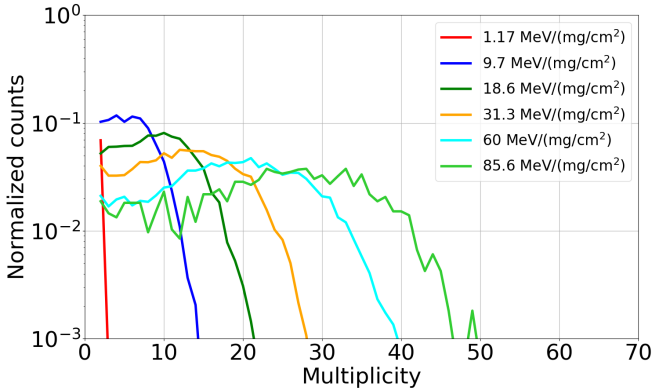

Fig. 4. Histogram of ion multiplicity for the MCUs collected with the beams at RADEF.

IV. LET DETERMINATION FROM MCUS

MCUs can be primarily classified through their multiplicity, i.e., how many bits in a cluster are in upset. The tight packing of cells within this SRAM allows reaching multiplicities as high as 50 when the LET of the ion is higher than 60 MeV/(mg/cm^2). One way to represent these data is through histograms of probability that an MCU for that ion beam will have a certain multiplicity. This is shown in Fig. 4 for the data collected at RADEF, which span the largest LET range among the facilities in which data were collected. This same plot for the data collected at UMCG-PARTREC, GANIL and GSI was already published [31]. Here only RADEF data are proposed because they make the figure more readable and, as said, they provide a full picture for an LET range going from ∼1 to ∼90 MeV/(mg/cm^2). Note that the plot only shows MCUs, so no data for single-bit upsets are reported, although they were included in the normalization.

Concerning the data in the figure one can notice that the maximum possible multiplicity of the MCUs becomes increasingly larger with increasing LET. For ions with LETs as low as 1 MeV/(mg/cm^2) MCUs with multiplicity of 2 occur less than once every ten ion strikes. From all the histograms, one can see that the probability of an ion causing an MCU with multiplicity of 2 or maximum multiplicity is more or less identical. Rather than in a peak, the data seem to distribute around a flat-top of equal likelihood that is followed by a fall-off at high LET. This result is different from what was observed before [40, 41] where the MCU distribution had a clear Gaussian-like peak distribution with increasing LET.

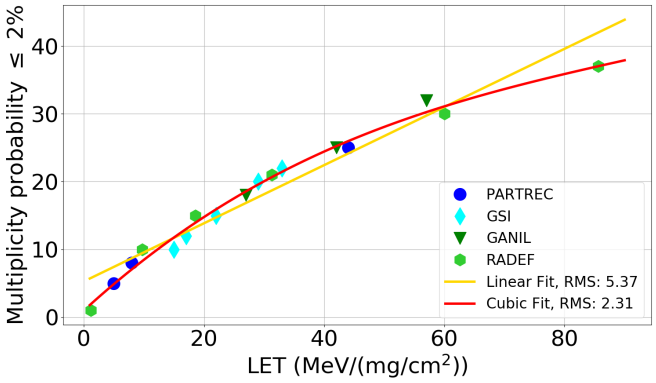

Fig. 5. 0.02-intercept of the MCU probability distributions as a function of LET and corresponding linear and cubic fits.

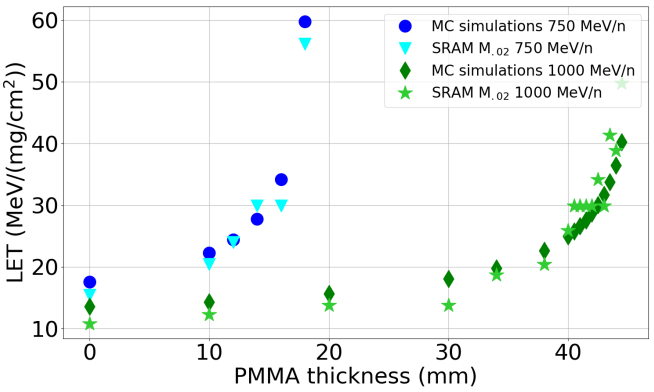

Fig. 6. Comparison between LETs estimated with FLUKA MC and those determined from the SRAM MCUs with the $M_{.02}$ parameter for different ion beam primary energies and at varying thickness of PMMA degrader.

The absence of a net peak for a certain LET complicates the task of estimating the LET of the beam from these distributions. In fact, MCUs with multiplicity of, e.g., 20, are possible with any ion having LET from 18 to 86 MeV/(mg/cm^2). Therefore, one can use information related to the whole distribution to estimate the beam LET.

It stands out that the maximum possible multiplicity increases with the LET in a rather regular fashion. An information like the intercept for a certain given probability can carry the information related to the maximum possible multiplicity for a certain LET. For instance, the multiplicity at which the histogram for each LET becomes lower than 0.01 or 0.02 can be determined and plotted as a function of the LET. This gives the data-points in Fig. 5 where the data for all the facilities are shown.

It must be noted that this parameter may be affected by strong uncertainty because it requires collecting a considerable amount of statistics in terms of MCUs for those multiplicities for which the occurrence probability starts being extremely low. As a result and considering that for the oldest measurements collecting MCUs was not within the purpose of the measurements, some data-points in the histograms may not be well behaved or fully monotonic. The RADEF data at all LETs up to 60 MeV/(mg/cm^2) have the highest statistics and, as such, can be considered the most reliable and the most well-behaved. On the other hand, the histogram for 85.6 MeV/(mg/cm^2) has some shaky shape and can have small relative peaks within the fall-off at high multiplicity. The 0.02-intercept is chosen over the 0.01-intercept because it provides more robust information over these uncertainties. This value is hereafter called $M_{.02}$.

When all the data are put together, and in particular when RADEF data are considered, i.e., single facility with the same device for the broadest LET range, it is clear that these points are sub-linearly correlated with the LET. A cubic fit provides a better approximation than a linear fit for all the points and seems to follow very well the RADEF points at any LET from 1 to 90 MeV/(mg/cm^2). The cubic fit here proposed follows the law below and will be solved for LET:

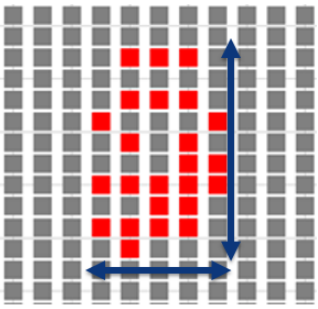

Fig. 7. Example of a cluster with multiplicity of 24 with indication of the δx and δy dimensions.

$$M_{.02} = 2.32 \times 10^{-5} \times LET^3 - 6.54 \times 10^{-3} \times LET^2 + 0.81 \times LET + 0.98 \quad (3)$$

To test this method, the data collected from the high-energy heavy ion facility HEARTS@CERN with primary and degraded beams are used. Currently, in this facility the beam LET is determined through FLUKA Monte-Carlo simulations incorporating all the material budget in the beamline, which include tens of meters of air as well as PMMA degrader slabs of several tens of mm.

Fig. 6 displays this comparison for several data-points collected from two primary Pb ion energies of 750 and 1000 MeV/n and with varying PMMA thickness. The more PMMA is inserted in the beam the closer the ions get to the Bragg peak. Overall, the plot shows a good qualitative agreement at both low and high LET, however, the method tends not to capture too well slight variations in the LET, returning for several points the same exact LET in spite of variations of ~5 MeV/(mg/cm^2). Also due to the uncertainties in determining $M_{.02}$, slight non-monotonic predictions may occur.

A second method is proposed that starts from the analysis of different parameters characterizing the MCUs. Other than the multiplicity, i.e., the number of bit flips, the MCUs can also be classified by their extension in horizontal and vertical direction. As can be seen in Fig. 7, the large MCUs in this

SRAM are not often condensed around the ion strike, but the bit-flips can have a rather random arrangement. One can define the size of the MCU in horizontal (bit-line) and vertical (word-line) direction through the δx and δy parameters.

This provides the chance to analyse the MCU in a 2-dimensional space that considers these two parameters. One can then plot normalized histograms of probability of occurrence of MCUs based on the combinations of δx-δy pairs. Such a 2D histogram can be better represented with heatmaps such as those in Fig. 8. These heatmaps are those generated from the MCU data available from the six reference RADEF ions. These heatmaps provide histogram distributions that have more marked characteristics than the histogram for the multiplicity alone. In fact, a clear hotspot is visible in all the figures showing that ions of a certain LET are more likely to induce MCUs having a restricted number of combinations of δx and δy. This hotspot also moves to higher and higher δx and δy as the LET of the beam is increased.

Nevertheless, the hotspot alone does not vary so much as to provide a sufficiently precise discrimination for the LET of the beam. Therefore, methods that better exploit all the information contained in the heatmap can be identified. Heatmaps similar to these will be produced by beams of which the LET is not known. A similarity algorithm among heatmaps can be constructed that can provide an estimation of the LET based on a difference minimization technique among the known calibration heatmaps. For this method, the principle is based on calculating the Root Mean Square (RMS) difference between the new heatmap for which one wants to determine the LET of the beam and all the calibration heatmaps. The RMS_i with respect to each i^{th} calibration heatmap is calculated taking into account all points in the heatmaps, with $\mathrm{P}_{\Delta x_j,\Delta y_k,Z}$ indicating the probability values reported in each point of the heatmaps in Fig. 8 for the various pairs of Δx and Δy, and Z indicating whether it is the heatmap of one of the calibration runs (calib_i) or that for which the LET has to be determined (LET?):

$$RMS_i = \sqrt{\sum_j \sum_k (P_{\Delta x_j,\Delta y_k,calib_i} - P_{\Delta x_j,\Delta y_k,LET?})^2} \tag{4}$$

Once these values are calculated, to determine the LET, the proposed method consists in collecting the five points that have the minimum RMS_i and then apply a weighted sum of the LET of these calibration point. These weights are nothing but the reciprocal of the RMS_i, so that more importance is given to the LETs that are expected to be the closest to the correct value and normalizing the result with respect to the sum of these weights.

$$LET = \frac{\sum_i RMS_i^{-1} \times LET_i}{\sum_i RMS_i^{-1}} \tag{5}$$

This method is also tested in the same fashion as the previous one and the comparison between these estimations and those from FLUKA are reported in Fig. 9. Also in this case the agreement is qualitatively good. In addition, this method better captures slight increases of LET and it provides fully monotonic data with increasing PMMA thickness.

Overall the two methods achieve very similar accuracy. A detailed plot of the difference in terms of LET for each data-point between FLUKA simulations and the values obtained from the SRAM with the two methods is available in Fig. 10. The differences increase when small variations in the thickness cause large variations of the LET, i.e., when getting closer to the Bragg peak. The first method has an average discrepancy with respect to the points calculated with the Monte-Carlo simulation of 3.01 MeV/(mg/cm^2), whereas the second has an average discrepancy of 3.66 MeV/(mg/cm^2). Note that these accuracies are calculated with respect to a FLUKA simulation, so this may as well be affected by uncertainty. Both methods seem to provide better estimations for the cases in which the beam is degraded from 750 MeV/n than when it is degraded from 1000 MeV/n.

V. Conclusions

The paper presents MCU data on an SRAM collected in various European heavy ion facilities. The MCU data are used to enhance the capability of SRAMs as heavy ion beam detectors. The main two enablers provided by MCUs are:

- The possibility to have a flux measurement that is independent with respect to the knowledge of the LET of the beam, limited to LET $>$ 10 MeV/(mg/cm^2).
- The determination of the LET of the heavy ion beam with rather small uncertainty and without having any other knowledge arising from other instruments.

Concerning the first point, the concept of coverage to compare the number of MCUs and the ion fluence is introduced. It is shown that, differently from the SEU cross section, this paramater fully saturates at LET $>$ 10 MeV/(mg/cm^2). Therefore, a simple formula that takes into account the geometrical characteristics of the sensitive surface can be used to estimate the flux even when the LET of the beam is not known with precision. This method was tested against some measurements performed at facilities, which pointed out potential shortcomings in the determination of the fluence of the facility. In some cases, re-calibrations of the ion counts were performed by the facility that returned the correct saturation value.

Concerning the second point, statistics about the multiplicities or the shapes of the MCUs as a function of the LET can be used to obtain an estimation of the LET of the beam. A first method that relies solely on the multiplicity is proposed. This is based on determining the 0.02-intercept of the multiplicity distributions of each ion and by performing a cubic fit with the LET. Solving the equation for LET from the 0.02-intercept of a beam of unknown LET returns the estimated LET of this beam with an accuracy of about 3 MeV/(mg/cm^2). A similar accuracy is obtained when using a method that makes use of 2D distributions of the sizes of the MCUs and by RMS of the various distributions with one another.

It is worth mentioning that these results on the LET and flux estimation at HEARTS@CERN were obtained with less than 10^4 ions/cm^2 total fluences per ion run on the SRAM. Therefore, the dose received by the SRAM is extremely small

This article has been accepted for publication in IEEE Transactions on Nuclear Science. This is the author's version which has not been fully edited and content may change prior to final publication. Citation information: DOI 10.1109/TNS.2024.3487647

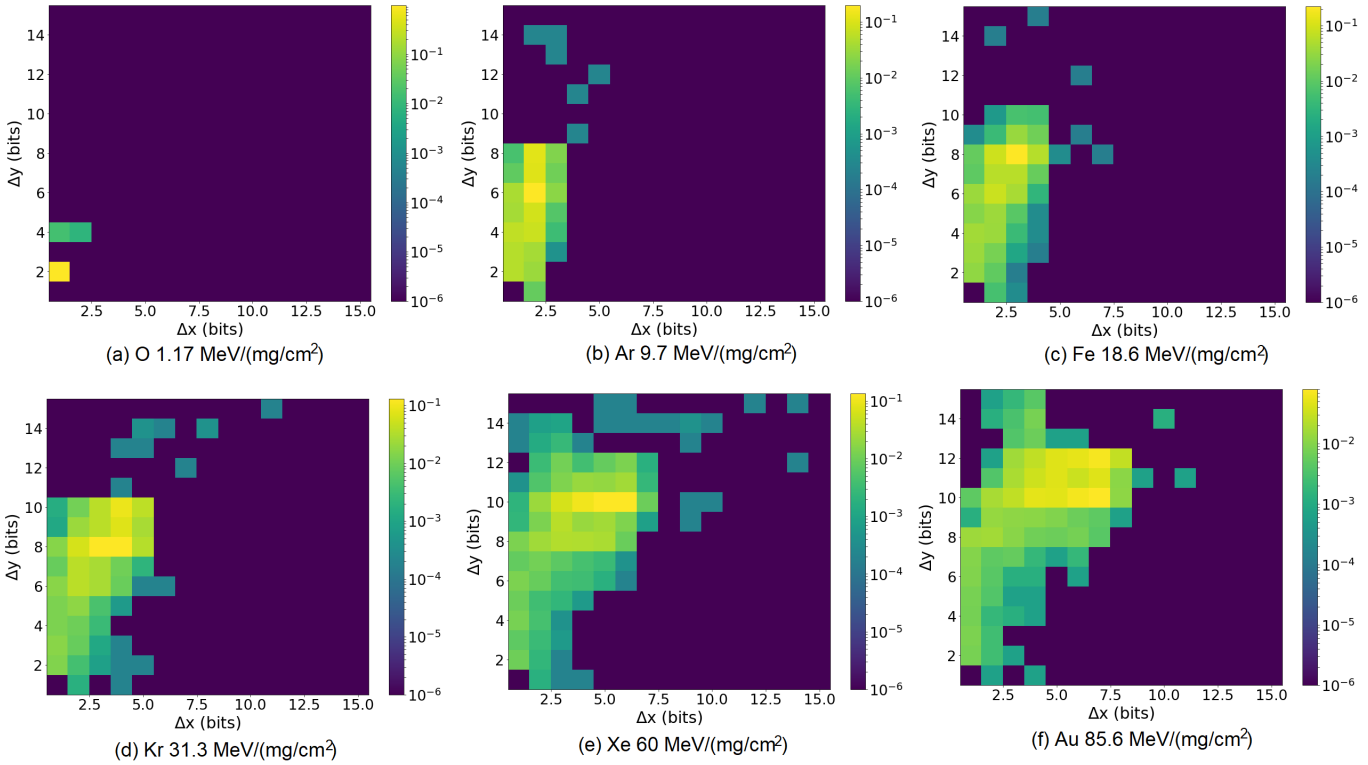

Fig. 8. Heatmaps of MCU clusters based on the combinations of Δx-Δy for the data collected at RADEF. The colorbar indicates the probability that an MCU will have a certain combinations of Δx-Δy with respect to the total number of MCUs.

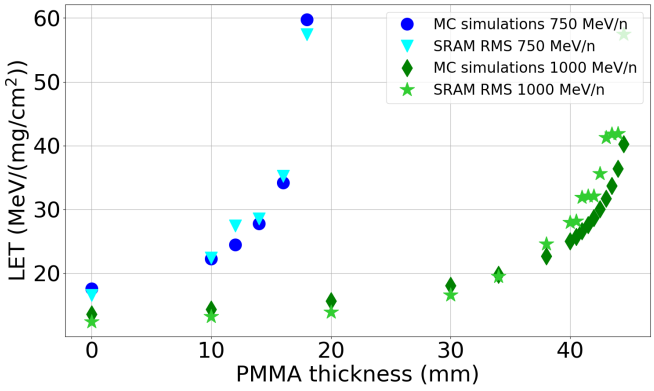

Fig. 9. Comparison between LETs estimated with FLUKA MC and those determined from the SRAM MCUs with the RMS-based method for different ion beam primary energies and at varying thickness of PMMA degrader.

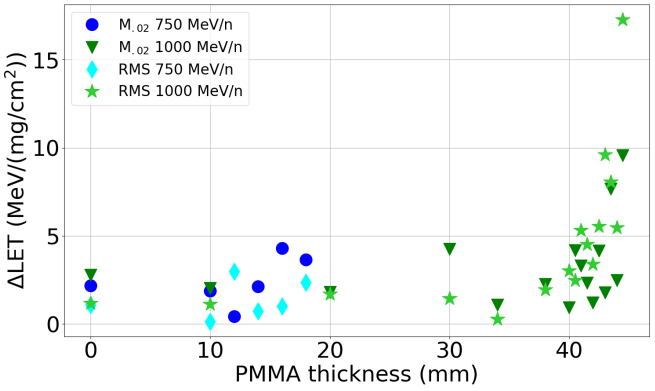

Fig. 10. Difference between the FLUKA simulated LETs and those retrived with the SRAM with the two methods as a function of thickness and primary energy of the ion.

(a few rads depending on the ion LET) and no impact from total ionizing dose on SEU sensitivity is expected for several hundreds of thousands runs.

The work here reported was paramount in having an estimation of the accuracy of the dosimetry at HEARTS@CERN during the pilot run in 2023. In fact, the SRAM allowed determining the LET and flux of the beam during the run itself, when most of these parameters were not yet calibrated with instruments at the facility or the LET had not been obtained by MC simulations.

VI. Acknowledgments

We acknowledge Helmut Puchner from Infineon for disclosing the information required to disable the embedded error correction code in the CY62167GE30-45ZXI and for providing the logical-to-physical descrambling information for the memory.

We acknowledge Heikki Kettunen, Mikko Rossi, Jukka Jaatinen, Kimmo Niskanen, Arto Javanainen from RADEF, Marc-Jan Van Goethem, Harry Kiewiet, Brian Jones and Sytze Brandenburg from UMCG-PARTREC, Marie-Helene Moscatello and Antoine Dubois from GANIL, Tim Wagner, Christoph Schuy, Kay Obbe Voss and Marco Durante from

GSI, Natalia Emriskova, Eliott Johnson and Matthew Fraser from CERN for their help during data collection.

VII. Data access

The MCU data used for this work are available on Zenodo at the following DOI: https://doi.org/10.5281/zenodo.8314389.

References

[1] G. Tsiligiannis et al., "An SRAM based monitor for mixed-field environments," *IEEE Trans. Nucl. Sci.*, vol. 61, no. 4, pp. 1663-1670, Aug. 2014.

[2] F. Spiezia et al., "A new RadMon version for the LHC and its injector lines," *IEEE Trans. Nucl. Sci.*, vol. 61, no. 6, pp. 3424-3431, Dec. 2014.

[3] J. Prinzie et al., "An SRAM-based radiation monitor with dynamic voltage control in 0.18 μm CMOS technology," *IEEE Trans. Nucl. Sci.*, vol. 66, no. 1, pp. 282-289, Jan. 2019.

[4] J. Wang, J. Prinzie, A. Coronetti, S. Thys, R. García Alía, P. Leroux, "Study of SEU sensitivity of SRAM-based radiation monitor in 65-nm CMOS," *IEEE Trans. Nucl. Sci.*. vol. 68, no. 5, pp. 913-920, May 2021.

[5] R. Harboe-Sorensen et al., "From the reference SEU monitor to the technology demonstration module on-board PROBA-II,"*IEEE Trans. Nucl. Sci.*, vol. 55, no. 6, pp. 3082-3087, Dec. 2008.

[6] R. Harboe-Sorensen et al., "The technology demonstration module on-board PROBA-II," *IEEE Trans. Nucl. Sci.*, vol. 58, no. 3, pp. 1001-1007, June 2011.

[7] F. Bezerra, R. Ecoffet, E. Lorfèvre, A. Samaras, and C. Deneau, "CARMEN2/MEX: an in-flight laboratory for the observation of radiation effects on electronic devices," *in Proc. 2011 RADECS Conf.*, Seville, Spain, Sept. 2011, pp. 607-614.

[8] A. Samaras, F. Bezerra, E. Lorfèvre, and R. Ecoffet, "CARMEN-2: in flight observation of non-destructive single event phenomena on memories," *in Proc. 2011 RADECS Conf.*, Seville, Spain, Sept. 2011, pp. 839-848.

[9] A.L. Bogorad, J.J. Likar, R.E. Lombardi, S.E. Stone, and R. Herschitz, "On-orbit error rates of RHBD SRAMs: comparison of calculation techniques and space environmental models with observed performance," *IEEE Trans. Nucl. Sci.*, vol. 58, no. 6, pp. 2804-2806, Dec. 2011.

[10] R. Harboe-Sorensen et al., "PROBA-II technology demonstration module in-flight data analysis," *IEEE Trans. Nucl. Sci.*, vol. 59, no. 4, pp. 1086-1091, Aug. 2012.

[11] M. D'Alessio et al., "SRAMs SEL and SEU in-flight data from PROBA-II spacecraft," *in Proc. 2013 RADECS Conf.*, Oxford, UK, Sept. 2013, pp. 91-98.

[12] B. D. Sierawski et al., "CubeSats and Crowd-Sourced Monitoring for Single Event Effects Hardness Assurance," *IEEE Trans. Nucl. Sci.*, vol. 64, no. 1, pp. 293-300, Jan. 2017.

[13] D. Alexander et al., "Single event upset results from the radiation hardened electronic memory experiment on the International Space Station," *in IEEE Radiation Effects Data Workshop Rec.*, Waikoloa, HI, July 2018, pp. 131-135.

[14] D. Alexander et al., "Single event upset results from the radiation hardened electronic memory experiment in a polar orbit," *in IEEE Radiation Effects Data Workshop Rec.*, Santa Fe, NM, July 2020, pp. 35-38.

[15] N. Kerboub et al., "Comparison between in-flight SEL measurement and ground estimation using different facilities," *IEEE Trans. Nucl. Sci.*, vol. 66, no. 7, pp. 1541-1547, July 2019.

[16] M. Pinto, P. Gonçalves, J. Sampaio, T. Sousa, C. Poivey, "CTTB memory test board single event effect geostationary in-flight data analysis", *in Proc. 2020 RADECS Conf.*, Vannes, France, Oct. 2020, pp. 165-170.

[17] J.J. Likar et al., "Initial in-flight error rates for 16-Mb SRAM as flying on the double asteroid redirection test (DART) mission," *IEEE Trans. Nucl. Sci.*, vol. 70, no. 4, pp. 426-433, Apr. 2023.

[18] F. Bezerra et al., "14 years of in-flight experimental data on CARMEN-MEX," *IEEE Trans. Nucl. Sci.*, vol. 70, no. 8, pp. 1533-1540, Aug. 2023.

[19] D. Alexander et al., "Single event upset results from the radiation hardened electronic memory experiment in a geostationary orbit," *in IEEE Radiation Effects Data Workshop Rec.*, Kansas City, Mo, July 2023, pp. 230-233.

[20] V. Wyrwoll et al., "Pulsed electron beam induced SEU effects in an SRAM memory", *in Proc. of 2021 RADECS Conf.*, Vienna, Austria, Sept. 2021, pp. 25-31.

[21] A. Coronetti, N. Emriskova, R. García Alía, J.A. Vera Sanchez, A. Mazal, "Assessment of the Quirónsalud proton therapy centre accelerator for single event effects testing," *IEEE Trans. Nucl. Sci.*, vol. 71, no. 8, pp. 1571-1579, Aug. 2024.

[22] G. Gasiot, D. Giot, and P. Roche, "Multiple cell upsets as the key contribution to the total SER of 65 nm CMOS SRAMs and its dependence on well engineering," *IEEE Trans. Nucl. Sci.*, vol. 54, no. 6, pp. 2468-2473, Dec. 2007.

[23] Y.-P. Fang and A.S. Oates, "Characterization of single bit and multiple cell soft error events in planar and FinFET SRAMs," *IEEE Trans. Dev. Mat. Rel.*, vol. 16, no. 2, pp. 132-137, June 2016.

[24] T. Kato et al., "The impact of multiple-cell charge generation on multiple-cell upset in a 20-nm bulk SRAM," *IEEE Trans. Nucl. Sci.*, vol. 65, no. 8, pp. 1900-1907, Aug. 2018.

[25] T. Kato, T. Yamazaki, N. Saito, and H. Matsuyama, "Neutron-induced multiple-cell upsets in 20-nm bulk SRAM: angular sensitivity and impact of multiwell potential perturbation," *IEEE Trans. Nucl. Sci.*, vol. 66, no. 7, pp. 1381-1389, July 2019.

[26] D. Giot, P. Roche, G. Gasiot, J.-L. Autran, and R. Harboe-Sorensen, "Heavy ion testing and 3D simulations of multiple cell upset in 65nm standard SRAMs," *Proc. RADECS Conf.*, Deauville, France, 2007, pp. 158-163.

[27] J.A. Clemente, G. Hubert, M. Rezaei, F.J. Franco, and H. Mecha, "Impact of the bitcell topology on the multiple-cell upsets observed in VLSI nanoscale SRAMs," *IEEE Trans. Nucl. Sci.*, vol. 68, no. 9, pp. 2383-2391, Sept. 2021.

[28] A. Virtanen, R. Harboe-Sorensen, A. Javanainen, H. Kettunen, H. Koivisto, and I. Riihimaki, "Upgrades for the RADEF facility," *in IEEE Radiation Effects Data Workshop Rec.*, Honolulu, HI, USA, July 2007, pp. 38-41.

[29] E.R. van der Graaf, R.W. Ostendorf, M.J. van Goethem, H.H. Kiewiet, M.A. Hofstee, and S. Brandenburg, "AGORFIRM, the AGOR facility for irradiations of material," *in Proc. 2009 RADECS Conf.*, Bruges, Belgium, Sept. 2009, pp. 451-454.

[30] M.-H. Moscatello, A. Dubois, and X. Ledoux, "Industrial applications with GANIL SPIRAL2 facility," *Proc. RADECS Conf.*, Bremen, Germany, 2016, pp. 313-315.

[31] R. Garcia Alia, A. Coronetti, K. Bilko, M. Cecchetto, G. Datzmann, S. Fiore, and. S. Girard, "Heavy ion energy deposition and SEE intercomparison within the RADNEXT irradiation facility network," *IEEE Trans. Nucl. Sci.*, vol. 70, no. 8, pp. 1596-1605, Aug. 2023.

[32] K. Bilko et al., "CHARM high-energy ions for micro electronics reliability assurance (CHIMERA)," *IEEE Trans. Nucl. Sci.*, vol. 71, no. 8, pp. 1549-1556, Aug. 2024.

[33] A. Coronetti et al., "SEU characterization of commercial and custom-designed SRAMs based on 90-nm technology and below," *in IEEE Radiation Effects Data Workshop Rec.*, Santa Fe, NM, USA, Dec. 2020, pp. 56-63.

[34] G. Battistoni et al., "Overview of the FLUKA code," *Annals of Nuclear Energy*, vol. 82, pp. 10-18, August 2015.

[35] T.T. Bohlen et al., "The FLUKA Code: Developments and Challenges for High Energy and Medical Applications," *Nuclear Data Sheets*, vol. 120, pp. 211-214, June 2014.

[36] C. Ahdida et al., "New capabilities of the FLUKA multi-purpose code," *Front. Phys.*, vol. 9, Art. no. 788253, Jan. 2022.

[37] A. Waets et al., "Very-high energy heavy ion beam dosimetry using solid state detectors for electronics testing," *IEEE Trans. Nucl. Sci.*, vol. 71, no. 8, pp. 1837-1845, Aug. 2024.

[38] G. Tsiligiannis et al., "Multiple cell upset classification in commercial SRAMs," *IEEE Trans. Nucl. Sci.*, vol. 61, no. 4, pp. 1747-1754, Aug. 2014.

[39] A. Bosser et al., "Investigation on MCU clustering methodologies for cross-section estimation of RAMs," *IEEE Trans. Nucl. Sci.*, vol. 62, no. 6, pp. 2620-2626, Dec. 2015.

[40] G.I. Zebrev et al., "Statistics and methodology of multiple cell upset characterization under heavy ion irradiation," *Nucl. Instr. and Meth. in Phys. Res. A*, vol. 775, pp. 41-45, Mar. 2015.

[41] G.I. Zebrev and K.S. Zemtsov, "Multiple cell upset cross-section modeling: a possible interpretation for the role of the ion energy-loss straggling and Auger recombination," *Nucl. Instr. and Meth. in Phys. Res. A*, vol. 827, pp. 1-7, Aug. 2016.